

ON-GROUND HVI ON A NANOSATELLITE. IMPACT TEST, FRAGMENTS RECOVERY AND CHARACTERIZATION, IMPACT SIMULATIONS.

Hakim ABDULHAMID⁽¹⁾, Dylan BOUAT⁽¹⁾, Anthony COLLÉ⁽²⁾, Jonathan LAFITE⁽³⁾, Jérôme LIMIDO⁽²⁾, Iko MIDANI⁽³⁾, Jean-Michel PAPY⁽³⁾, Christian PUILLET⁽⁴⁾, Martin SPEL⁽³⁾, Thomas UNFER⁽²⁾, Pierre OMALY⁽⁴⁾

⁽¹⁾ *THIOT Ingénierie, Route Nationale, 46130 Puybrun, France.*

abdulhamid@thiot-ingenierie.com ; bouat@thiot-ingenierie.com

⁽²⁾ *IMPETUS AFEA, 16 rue Isaac Newton, 31830 Plaisance-du-Touch, France.*

anthony@impetus.fr ; jerome@impetus.fr ; thomas@impetus.fr

⁽³⁾ *R.TECH, 10 impasse Jean Mermoz, Parc Technologique Delta Sud, 09340 Verniolle, France*

jonathan.lafite@rtech.fr ; iko.midani@rtech-engineering.com ; jean-michel.papy@rtech.fr ; martin.spel@rtech.fr

⁽⁴⁾ *CNES, 18 avenue Édouard Belin, 31401 Toulouse Cedex 9, France*

christian.puillet@cnes.fr ; pierre.omaly@cnes.fr

ABSTRACT

The development of nanosatellites raises the question of the evolution of risk posed by the increasing number of orbital debris to the sustainable use of space. In order to better understand and measure this increased risk, CNES' Tech4SpaceCare initiative granted an experimental and numerical study on the consequences of the catastrophic collision between a space debris and a nanosatellite.

For this purpose, a 0.845 kg nanosatellite was hit by a 0.72 g projectile launched at 6690 m/s (16.1 kJ). The fragments, down to approximately 1 mm in size, were recovered, measured (mass, lengths, area), recorded and stored. In parallel, a numerical simulation of the impact was performed and the fragments were identified, measured and recorded as well.

The paper presents the nanosatellite, the test set-up, the impact results and the numerical simulations. The results of the fragments measurements and the simulation of fragments generation are compared with NASA's satellite standard break-up model.

1 INTRODUCTION

The development of nanosatellites raises the question of the evolution of risk posed by the increasing number of orbital debris to the sustainable use of space. In order to better understand and measure this increased risk, CNES' Tech4SpaceCare initiative granted an experimental and numerical study on the consequences of the catastrophic collision between a space debris and a nanosatellite. This activity is in the line of previous collision tests [3, 4, 5] with an emphasis on the impact velocity.

The purpose of the work is to quantify the fragments generated by the impact, and to compare with an existing

model. Eventually this work will allow improvements of space debris environment evolution models and guide future strategies so as to ensure sustainable space activities.

The activities are organized in five steps:

- Procurement of the nanosatellite (§ 2)
- Hypervelocity impact tests (§ 3)
- Fragments recovery and identification (§ 4)
- Numerical simulation (§ 5)
- Test-simulation-models comparison (§ 6)

2 NANOSATELLITE PROCUREMENT

The nanosatellite was provided complimentary by the JANUS (now Nanolab-Academy) project, CNES' student's satellites project. The nanosatellite size was 150 mm * 100 mm * 100 mm and it weighted 845 grams. It contained actual but non-flight-acceptable parts, including a 4-cells battery pack, electronic boards, inertia wheels and a solar panel.



Figure 2-1. Nanosatellite

3 HYPERVELOCITY IMPACT TEST

The nanosatellite was delivered to THIOT Ingénierie that was in charge of the hypervelocity impact test.

A dedicated container was designed and built to capture the fragments and to visualize the impact (see also ref. [3] for instance). A preliminary hypervelocity impact tests was performed on a dummy target. This test allowed to define the structural junctions between the different faces of the container, especially to avoid explosion of the transparent parts (made of Plexiglas and polycarbonate plates). The container internal faces were covered by foam so as to protect the container and to allow collecting the fragments. Two layers were used: a 30 mm thick external layer of 150 kg/m³ polyurethane foam and a 30 mm thick internal layer of 30 kg/m³ polystyrene.

Figure 3-1 presents the nanosatellite in the container (impact on the side nr. 1) with eight steel cables to maintain the nanosat in place. The battery side was chosen to be the impact side.



Figure 3-1. Nanosatellite in the container

The container was placed in the impact chamber of the HERMES two-stage light-gas launcher.



Figure 3-2. HERMES launcher and its impact chamber, in black



Figure 3-3. Container in the impact chamber (projectile launched from the right side)

Two high-speed cameras were installed to record the impact, one on the side (see circular window on the left side of figure 3-3) and one on the top. The top side was not protected by foam.

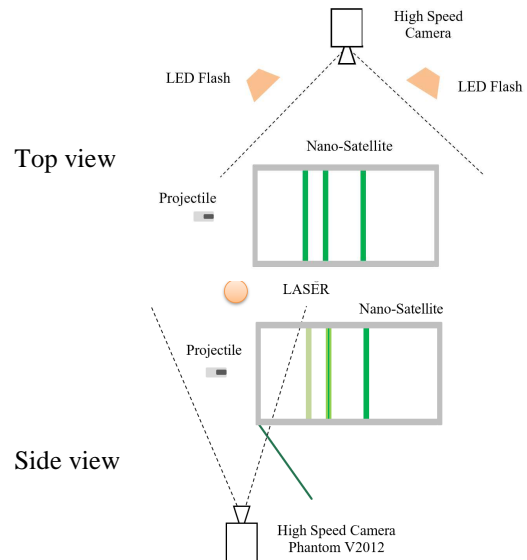


Figure 3-4. Cameras configuration

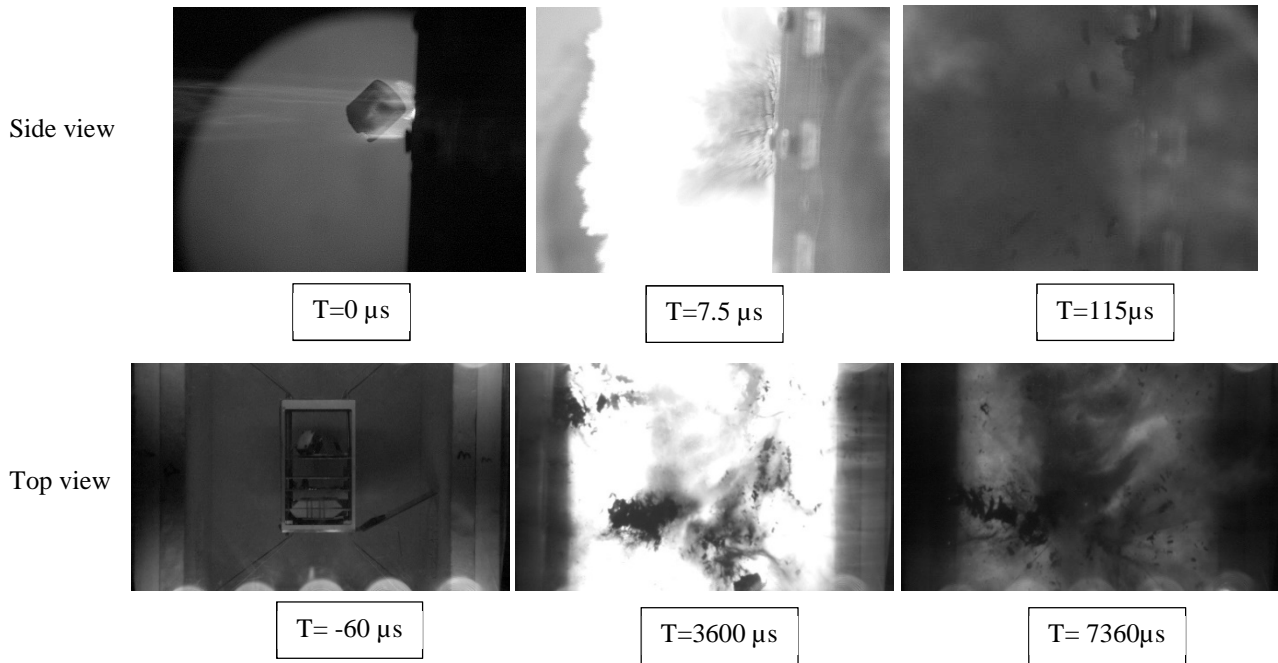
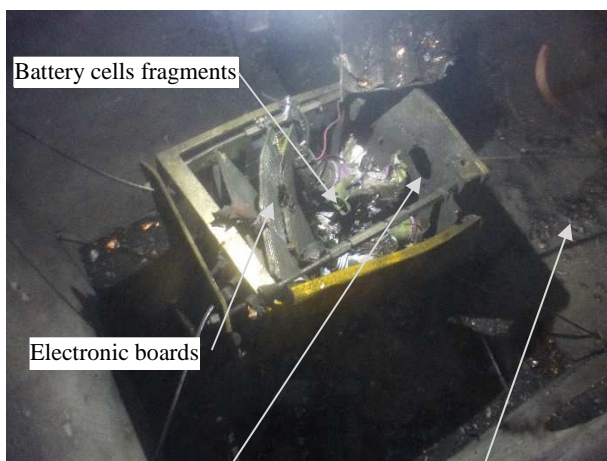


Figure 3-5. Images from high speed cameras impact

The 0.72 grams projectile was made of a cylindrical polycarbonate sabot (9 mm height and 9 mm diameter) with an embedded aluminium cylinder (4 mm height and 4 mm diameter). The impact test was performed on July 1st, 2020. The impact velocity was recorded at 6690 ± 50 m/s, to give a kinetic energy of 16.1 ± 0.24 kJ.

Fig. 3-5 shows some images of the impact event. The projectile reached the nanosat with an important tilt. A very high temperature gas was generated by the impact of the polycarbonate sabot on the aluminium front plate which oversaturates the camera sensor and partially conceals the fragment generation. Some fragments are observed from the top view at 3.5 ms after the impact.



Front plate perforation Retrojet debris impacts

Figure 3-6. Top view after impact

The energy-to-mass ratio of the impact test was 19 kJ/kg, i.e. approximately half the NASA's catastrophic impact threshold of 40 kJ/kg. This energy was not able to destroy the nanosatellite, but caused significant catastrophic damages and numerous fragments. The battery cells were destroyed and the electronic cards in the back were severely damaged. However, thanks to the battery pack protection, the primary structure remained complete.

The battery cells internal multilayers structure generated many small fragments, as shown below.



Figure 3-7. Detailed view of the battery cells after impact



Figure 3-8. View of fragments at the bottom of the container

Note that the battery pack is no longer fixed to the structure as shown in fig. 3-9 after transportation of the container.



Figure 3-9. Nanosat after transportation.

4 FRAGMENTS RECOVERY AND MEASUREMENTS

The container was then transferred to R.TECH that was in charge of the fragments recovery and measurements.

4.1 Fragments recovery

The fragments were either loose at the bottom of the container, or embedded into the foam. As the fragments were extracted, their location was recorded, in view of future use of the results. The fragments were extracted from the foam either mechanically or chemically.

For the mechanical extraction, it was found that the extraction from the external layer (polyurethane) was complex and tedious, whereas no fragment did actually completely perforate this polyurethane layer. For future tests at same kinetic energy, a less dense material could be used. The mechanical extraction from the polystyrene

layer was much easier.

For the chemical extraction, several polystyrene parts were dissolved into an acetone bath which allowed the fragments to fall down at the bottom of the tank.

The figures below present some extracted fragments.



Figure 4-1. Polystyrene part floating on an acetone bath.



Figure 4-2. Fragments recovered from the fig. 4-1 bath.



Figure 4-3. Large fragments.
(FGD = Fond Gros Débris)



Figure 4-4. Small fragments hidden in dust.

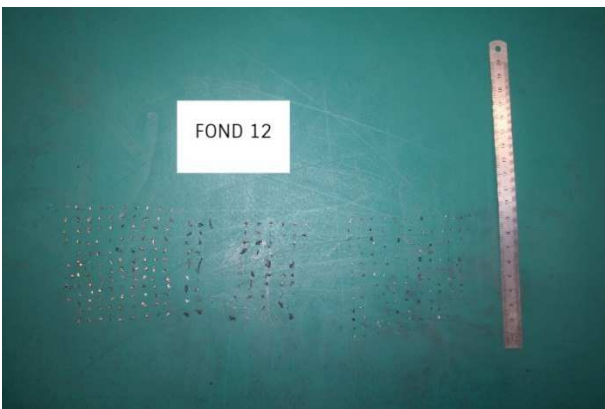


Figure 4-5. Small fragments recovered from fig. 4-4 dust.

In addition to the main structure and tiny loose parts, 1443 fragments were recovered, 70.90% of them were lying at the bottom of the container.

Location	1 st level (polyester)	2 nd level (polyurethane)
Bottom (1)	70.90%	3.13%
Left (2)	3.00%	0.54%
Right (3)	3.87%	0.41%
Top (4)	5.10%	N/A
Front (5)	6.53%	3.87%
Back (6)	2.65%	N/A

Table 4-1. Location of recovered fragments

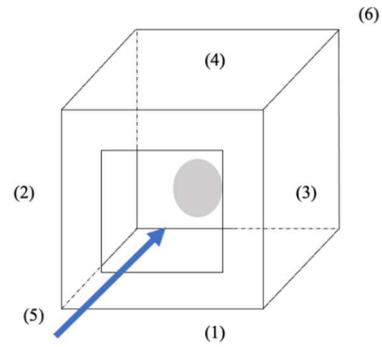


Figure 4-6. Definition of location for recovered fragments in the container

4.2 Fragments measurements

A dedicated set-up was defined to maximize the measurement automation. The most challenging issue was the automation of the weight measurement.

Each fragment is manually placed on a small cup uniquely identified by a datamatrix and previously weighed. A measurement cycle starts when a cup is detected at the entrance by a diffuse sensor [11]. A 6-axis industrial arm robot [12] takes the cup, scans its datamatrix using a 2D code reader [13] to take in account cup's weight, and puts it on a scale [14]. While the weight stabilizes, the fragment is scanned by a 3D Camera [15]. Then the arm robot replaces the cup and the fragment next to the operator who puts the debris on a small box where the operator will stick a QR Code tag printed [16]. The data are stored on a PostgreSQL database which is displayed in real time on a Human-Machine Interface. Cycle time average for one sample is 20.3 s.

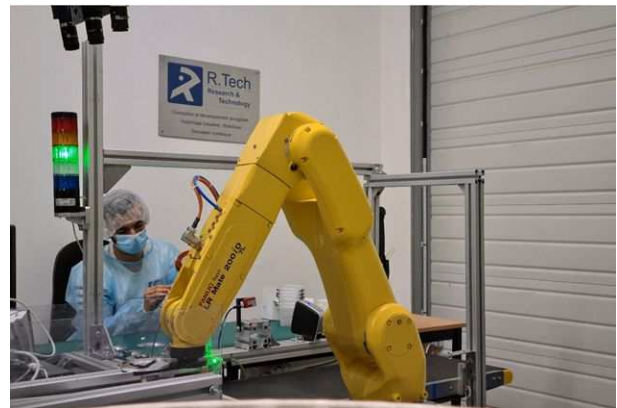


Figure 4-7. Overview of the measurement set-up

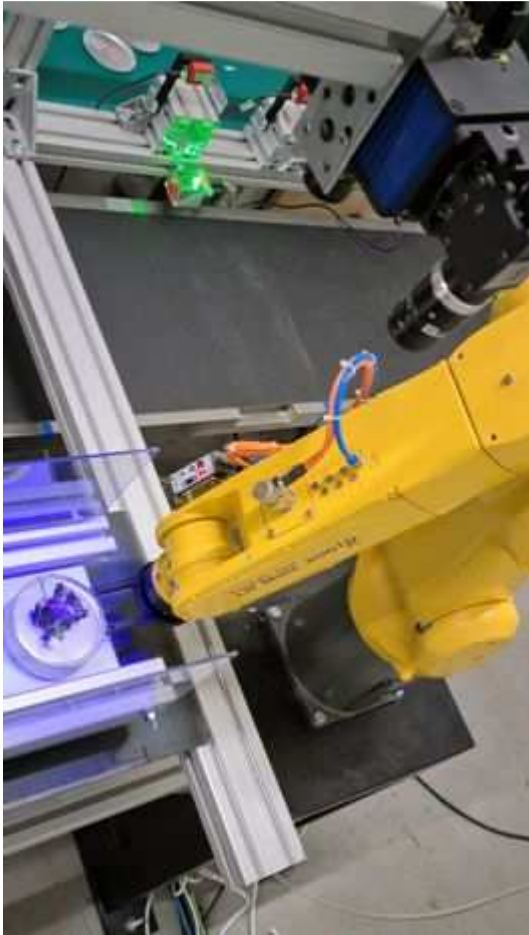


Figure 4-8. 3D camera shoot (blue light) while the fragment and cup are weighted.



Figure 4-9. Fragments departure and arrival spots.

The 3D images are defined as clouds of coordinates in 3D space and analysed to compute the fragments characteristic dimensions. After the shooting, data acquisitions include initially the fragment and his cup as shown on fig 4-10. Numeric treatments are necessary in order to extract the fragment from the point cloud and triangulate it.

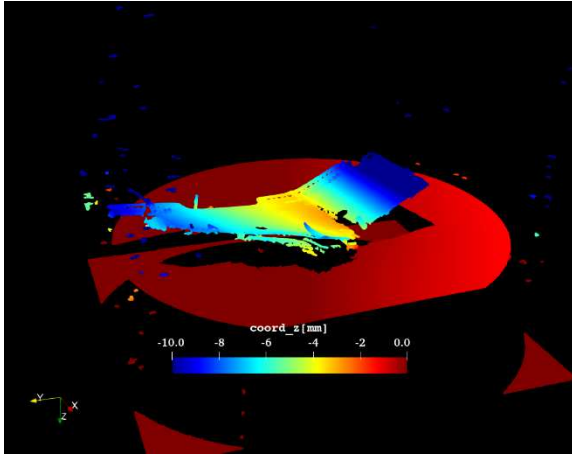


Figure 4-10. Raw image and fragment domain.

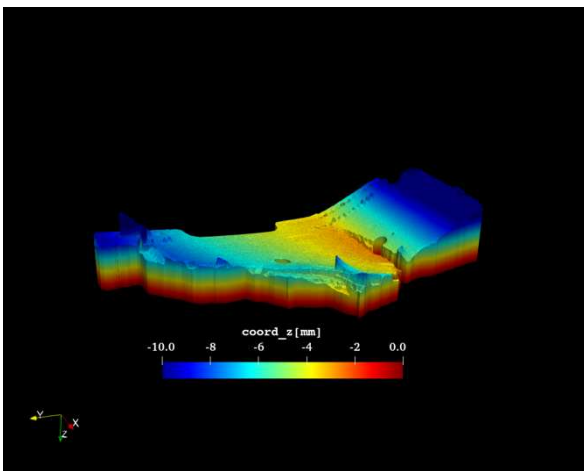


Figure 4-11. Image after triangulation.

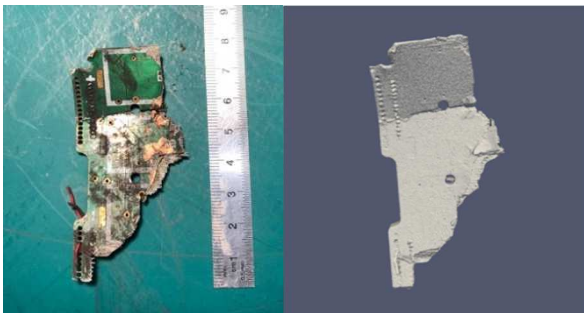


Figure 4-12. Recovered fragment(left), final meshing (right)

As it can be seen on fig. 4-11, the base of the fragment is not always well captured. Fortunately, this has generally limited impact on the characteristic length, and no impact on the mass as it is recorded independently. However, this prevents a density analysis, as the fragment volume is overestimated.

The characteristic length L_c is defined as the length average in each direction.

$$L_c = \frac{L_x + L_y + L_z}{3}$$

The first length is computed using the two most distant nodes defining the mesh. The other two are obtained in the same way, perpendicular to the first axis such as we can numerically define an oriented bounding box, see fig. 4-13.



Figure 4-13. Bounding box calculation in view of characteristic length calculation.

1411 out of the 1443 recovered fragments and the main structure could be measured (lengths and mass) in view to a comparison with simulation results and models.

The table below presents the mass summary: 96.6 % of the initial mass was retrieved, 93.7 % of the initial mass was measured.

Parts	Mass (g)
Main structure (1 fragment)	578.83
Collected fragments (1411 fragments measured)	212.96
Collected fragments (32 fragments not measured)	1.33
Metallic foils	1.62
Carbon/carbonized foils	9.03
Dust	12.46
Lost (not retrieved)	28.77
<i>Total (= initial mass)</i>	<i>845</i>

Table 4-2. Mass budget

5 IMPACT SIMULATION

While the fragments were extracted and measured, IMPETUS AFEA was in charge of the simulation of the impact.

The nanosatellite was modelled as a set of structural parts in Impetus Solver ®. In addition to common hypervelocity impacts simulations using Smooth Particles Hydrodynamics techniques, the fragments were individually recorded and characterized in size, mass and velocity. The characteristics lengths were computed so as to comply with NASA's satellite standard break-up model [1] (see also [7])

Fig. 5-1 presents the geometry of the nanosatellite. In view of the effects of the impact on the battery cells and the consequence in term of number of fragments, the initial idealization of the cells was refined and the different layers were roughly represented individually (see figure 5-2).

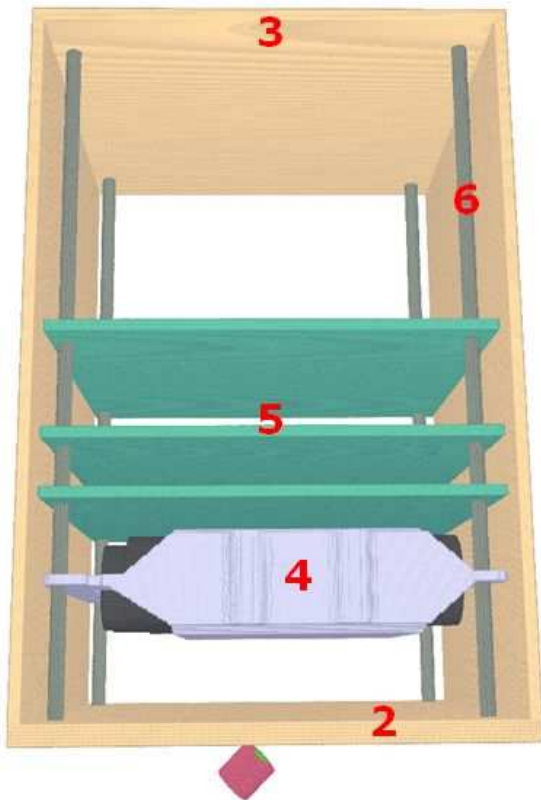


Figure 5-1. View of the SPH model

The impact is computed using the standard computational techniques with Gamma-SPH method and actual or estimated material properties, equations of state (such as Mie-Grüniesen), strength models (such as Johnson-Cook) and damage models (such as Cockcroft-Latham).

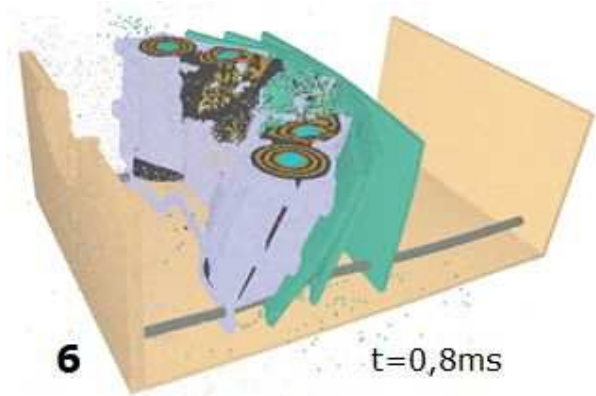


Figure 5-2. Impact simulation at time=0.8 ms (γ SPH method), lower half



Figure 5-3. Top view of plastic strain inside the structure (see also fig. 3-7 for inner impacts on the front face)

The computation time was 19 hours on a standard workstation with 1 GPU Nvidia ® P5000. This duration was later reduced down to 5 hours with a GPU Nvidia ® GeForce RTX 2080 Ti.

In order to reduce the computation time, a simplified model using a combination of Finite Elements Method and Discrete Elements Methods based on Lennard-Jones potential and empirical material parameters from impacts of aluminium spheres on aluminium plates from [2] was developed and tested.

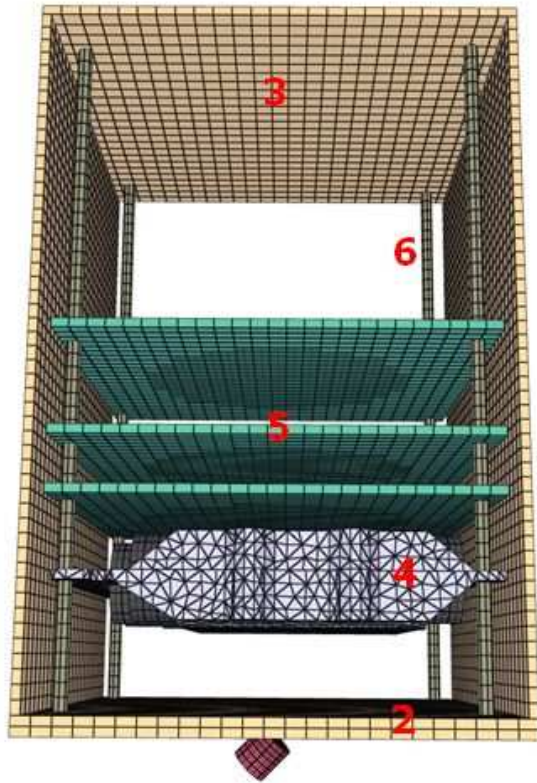


Figure 5-4. View of the DEM model

The computation time was reduced down to 6 h 20 minutes, taking also advantage of the coarse mesh. The global trends were comparable between both models, including the hole size. However, the simplified model could not capture local behaviour such as hailing (see fig. 3-6), the fasteners behaviour and small fragments generation.

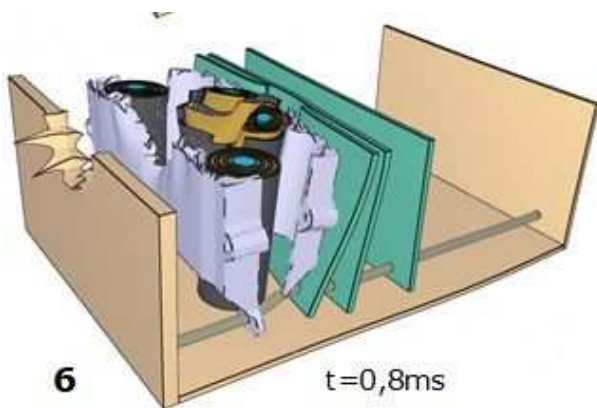


Figure 5-5. Impact simulation at time=0.8 ms (DEM method), lower half

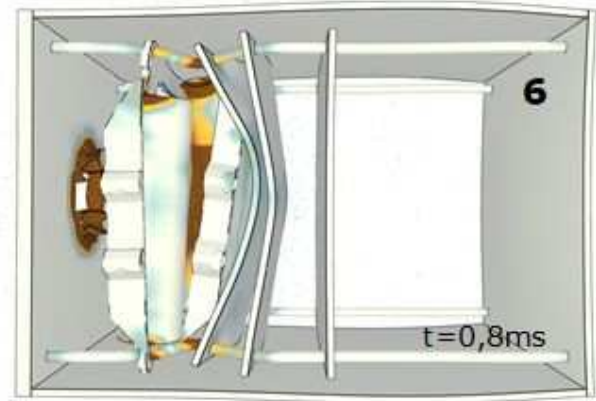


Figure 5-6. Top view of plastic strain inside the structure

Thanks to a reduced computation time, the simplified model can be useful to define the global kinematics of the impact but the fragments analysis requires the full model.

The list of generated fragments was defined at the end of the computation. A total of 771 fragments were recorded with coordinates, dimensions and characteristic length computed as defined in [1], mass and velocity in view to a comparison with tests results and models

6 TEST-SIMULATION-MODEL COMPARISON

The test and simulation results are compared with NASA satellite standard break-up model [1] as implemented in CNES' MEDEE orbital debris evolutionary model [8].

NASA's model assumes fragments characteristic length of 1 mm or more, and ensures mass conservation on this hypothesis [9]. For both test and simulation, there are fragments smaller in size. Therefore, the total mass considered will not be the same in all cases.

As it can be seen in fig. 5-1 for instance, the simulation model does not comprise all the parts. Some parts at the back of the nanosatellite, some parts of the electronic boards and the solar panel are not modelled. The modelled mass is 683 grams. 429 fragments (out of the 771 fragments computed) with characteristic length greater than 1 mm are considered with a total mass of 682.7 grams.

For the test results, 865 fragments (out of the 1412 recovered and measured) with characteristic length greater than 1 mm are considered with a total mass of 791 grams (out of 845 grams for the nanosatellite).

The parameters used for NASA's model are: use of the non-catastrophic impact collision model with spacecraft, mass of the target: 0.683 kg or 0.791 kg, mass of the projectile: 0.72×10^{-3} kg, impact velocity: 6.69 km/s. The number of generated fragments is typically 1027 (it does not depend on the target mass)

Fig 6-1 below plots the fragments distribution as a function of the characteristic length.

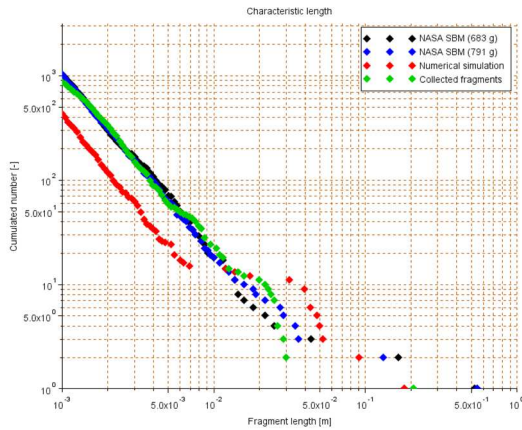


Figure 6-1. Fragments length distribution

The experimental data show a slope similar to NASA model, which is consistent with other experiments [3]. The number of small fragments is also very close to NASA’s model, much closer than expected in comparison with the results of ref. [3].

The numerical simulation uses only material physical properties and also shows a comparable slope. However, due to its limited representativeness, the number of fragments is lower.

Both the simulation and experimental data show the same trend for larger fragments (from the battery pack). However, the characteristic lengths of simulated fragments are larger. This will have to be analysed in future work.

Fig. 6-2 below plots the mass distribution as a function of the cumulated mass. The largest fragments of the simulation also appear as the heaviest fragments.

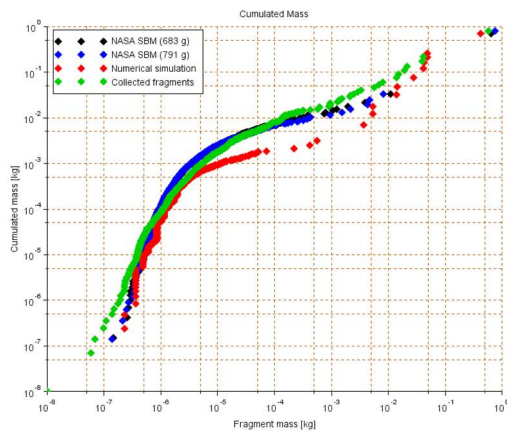


Figure 6-2. Fragments mass distribution

In the case of a non-catastrophic impact, NASA’s model defines two mass domain [9] “Non-catastrophic collision fragments are deposited from 1 mm upward until the total mass, $M = M_p * v_{imp}^2$, is achieved. The final fragment is deposited in a single massive fragment reminiscent of a cratered target mass.”. In this study, the mass limit $M_p * v_{imp}^2$ (velocity in km/s) is $0.72 * 6.69^2 = 32.2$ grams.

Green points (test data) in fig. 6-2 show that there are actually few fragments above this cumulated mass limit, originating mostly from the battery pack.

Fig. 6-3 below plots the Area over Mass ratio.

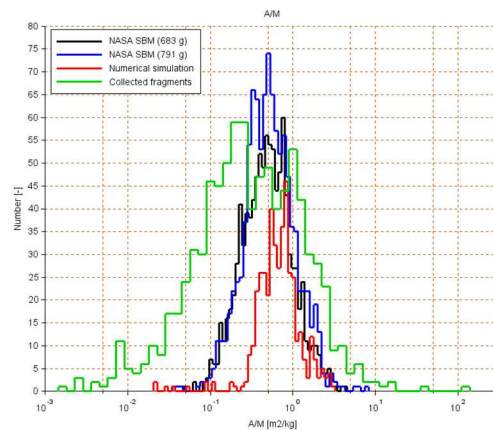


Figure 6-3. Fragments A/M distribution

For numerical simulation and collected fragments, the area was computed from the lengths as : $A = \frac{2}{9}(L_x L_y + L_y L_z + L_z L_x)$ (see [10])

The numerical simulation fragments have a slightly larger A/M ratio. The test results show a larger range of A/M values that NASA’s model. It is interesting to note that the test results seem to show two peaks. This kind of results was reported previously in ref. [3] and was associated to different materials: “the observed A/m distributions have two major peaks, corresponding to high- and low-density materials.”. Density analysis was not performed in this study; therefore, the detailed characteristics of the fragments is yet unknown. The results of such an analysis can also lead to the update of the numerical model with more modelled parts and more materials.

Fig. 6-4 below plots the velocities.

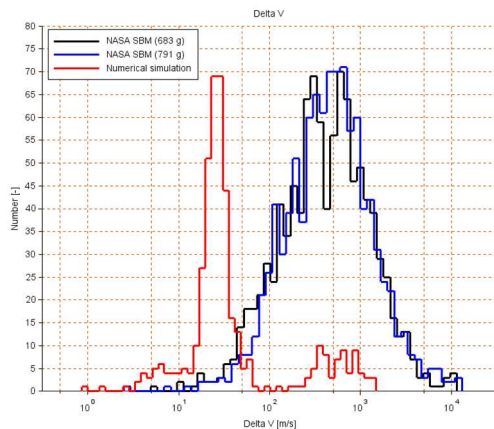


Figure 6-4. Fragments velocity distribution

The simulated velocities are one order of magnitude slower than the ones given by NASA’s model, except for retro-jet fragments. For this specific parameter, test results are barely exploitable. Further work is required to analyse this difference.

The test-simulation-model comparison shows generally rather close results (except velocity results) although some points need to be further analysed.

7 CONCLUSION

This paper presented the main steps of a on-ground hypervelocity impact test on a nanosatellite. The fragments were recovered and measured. In parallel, a numerical simulation was performed. The comparison of test results and numerical simulation with NASA’s break-up model shows rather close results (except some velocity results), and gives some directions for improvements.

These directions are as follows. For impact tests, improve the measurement of the fragments velocity. For fragments recovery and measurement, improve the geometrical definition of fragments and determine fragments average density. For numerical simulation, future work will have to focus on the two peaks aspects of the A/M ratio, on the velocity discrepancy with NASA model and on the total number of fragments.

8 ACKNOWLEDGMENT

The authors are grateful to the JANUS / Nanolab-Academy project team, headed by Mr. N. Verdier, and especially to Mr. S. Fredon for his involvement in the procurement of the nanosatellite.

9 REFERENCES

9.1 Documents

1. Johnson N.-L. et al., (2001) “NASA’s new breakup model of EVOLVE 4.0”, *Adv. Space Res.*, 28(9), pp. 1377-1384
2. Watson E. et al., (2017). “Discrete Particle Method for Simulating Hypervelocity Impact Phenomena”, *Materials* 2017, 10, 379; April 2017.
3. Hanada T. et al., (2009). “Micro-satellite Impact Testing”, 27th International Symposium on Space Technology and Science, Tsukuba, Japan, 2009
4. Lan S.-w. et al., (2014) “Debris area distribution of spacecraft under hypervelocity impact”, *Acta Astronautica* 105 (2014) 75–81
5. Cowardin H. et al., (2017). “Characterization of orbital debris via hyper-velocity laboratory-based tests”, 7th European Conference on Space Debris, Darmstadt, Germany, April 2017
6. Liou, J.-C. et al., (2014). “Successful Hypervelocity Impacts of DebrisLV and DebrisSat.” *Orbital Debris Quarterly News* 18(3), pp 3-6.
7. Collé, A. et al. (2021). “Innovative Meshless Approach for Hypervelocity Applications: Space Debris Impacts and Shaped Charges.” *Light-Weight Armour for Defence & Security (LWAG)*, October 19-20, Berlin, 2021 (to be confirmed).
8. Dolado-Perez, J.-C. et al., (2013). “Introducing MEDEE – a new orbital debris evolutionary model” 6th European Conference on Space Debris’, Darmstadt, Germany, 22–25 April 2013
9. Krisko, P. (2011). “Proper Implementation of the 1998 NASA Breakup Model” *Orbital Debris Quarterly News* 15(4), pp 4-5.
10. Hanada T, Liou J.-C (2011). “Theoretical and empirical analysis of the average cross-sectional areas of breakup fragments” *Advances in Space Research* 47 (2011) 1480-1489

9.2 Hardware

11. LEUZE HT25C/4P-M12 - Diffuse sensor with background suppression.
12. FANUC LR MATE 200id 7L arm robot.
13. LEUZE DCR 202i FIX-M1-102-R3 - Stationary 2D-code reader.
14. METTLER TOLEDO Weigh Module WXS205SDU/15.
15. Ensenso X36 3D camera system with FlexView2 technology.
16. SATO Printer WS412DT-DIS.